

Entanglement, anomalies and Mathisson's helices

Piermarco Fonda^{*1}, Diego Liska^{†2}, Álvaro Véliz-Osorio^{‡3}

¹ Instituut-Lorentz, Universiteit Leiden,
P.O. Box 9506, 2300 RA Leiden, The Netherlands

² Department of Physics, Universidad del Valle de Guatemala,
18 Avenida 11-95, Zona 15 Guatemala, Guatemala

³ M. Smoluchowski Institute of Physics, Jagiellonian University,
Łojasiewicza 11, 30-348 Kraków, Poland

Abstract

We study the physical properties of a length-torsion functional which encodes the holographic entanglement entropy for 1+1 dimensional theories with chiral anomalies. Previously, we have shown that its extremal curves correspond to the mysterious Mathisson's helical motions for the centroids of spinning bodies. We explore the properties of these helices in domain-wall backgrounds using both analytic and numerical techniques. Using these insights we derive an entropic c -function $c_{\text{Hel}}(\ell)$ which can be succinctly expressed in terms of Noether charges conserved along these helical motions. While for generic values of the anomaly there is some ambiguity in the definition of $c_{\text{Hel}}(\ell)$, we argue that at the chiral point this ambiguity is absent.

*fonda@lorentz.leidenuniv.nl

†lis14392@uvg.edu.gt

‡aveliz@gmail.com

Contents

1	Introduction and summary	2
2	Shape equations and anomalies	4
2.1	AdS ₃ helices	6
3	Holographic RG flows	8
4	Renormalized length-torsion functional	10
5	Mathisson helices: explicit parametrization	12
5.1	Helical motions: numerical solutions	15
6	Discussion and outlook	18
A	Helical Noether charges	19
B	Spinning-body charges in AdS₃	21
C	Holographic RG Flow Between 2d CFTs	22
D	Matching charges	23

1 Introduction and summary

Zamolodchikov's c -theorem [1] provides a deep insight into the general properties of quantum field theories. It states that for every Poincaré invariant local theory in two dimensions there exists a function of the couplings that decreases monotonically along renormalization group (RG) flows. Furthermore, if the theory in question is conformal, this function is constant and matches the central charge of the conformal field theory (CFT). This theorem formalizes the intuition that information regarding the microscopic details of the theory is lost as one studies it macroscopically, meaning that RG flows are irreversible. It is possible to generalize this result to chiral theories [2]: in this case, two distinct c -functions can be defined, one for left-movers and one for right-movers. As demonstrated in [2], the difference of these functions is constant along RG flows. This difference quantifies the number of degrees of freedom that are precluded from becoming massive at large distances. The fact that this quantity remains constant along the flow is a two-dimensional version of 't Hooft's anomaly matching condition for the chiral anomaly. In contrast, the sum of these functions decreases monotonically along the RG just as the non-chiral c -function.

It is well-known that there is an intimate relationship between gravity in AdS₃ and two-dimensional CFTs. Indeed, as discovered by Brown and Henneaux [3], the asymptotic

symmetry algebra for Einstein gravity in AdS₃ corresponds to a left- and a right-moving Virasoro algebra with identical central charges. In this work, we are interested in theories with chiral anomalies for which there is a mismatch between left- and right- moving central charges. On the gravity side, this is implemented by regarding AdS₃ as a solution of Topologically Massive Gravity (TMG) [4]. In this case, the difference between the central charges is proportional to the Compton wavelength of the massive graviton [5]. It has been argued that for arbitrary values of the graviton’s mass, TMG violates either unitarity or positivity [6]. However, at the critical point where the graviton’s Compton wavelength matches the AdS₃ radius these problems are absent. In this case, the dual central charges read

$$(c_L, c_R) = (0, 3L/G_3) , \tag{1.1}$$

where L is the AdS₃ radius and G_3 is the three-dimensional Newton’s constant. Condition (1.1) is known as the chiral point and the theory associated with it, called chiral gravity, has BTZ black holes and gravitons with non-negative mass [6].

The physics of RG flows can be probed using quantum information theoretical quantities such as entanglement entropy (EE). For 1+1 dimensional quantum field theories, it is well-known that the EE of a spacelike interval of length ℓ exhibits logarithmic divergences. Nonetheless, it is possible to extract its universal part by computing the *renormalized entanglement entropy* (REE) [7, 8]

$$\widehat{S}_{EE}(\ell) = \ell \frac{d}{d\ell} S_{EE}(\ell) . \tag{1.2}$$

If the field theory in question is conformal then the REE is proportional to the central charge and for a RG flow interpolating between two CFTs it was shown by Casini and Huerta [7] that (1.2) interpolates monotonically between their respective central charges, a result which furnishes an *entropic* proof of Zamolodchikov’s c -theorem. This story has a gravitational counterpart: it was shown by Ryu and Takayanagi (RT) [9] that calculating entanglement entropy (EE) for field theories with a dual gravitational description involves finding a suitable extremal surface in an asymptotically AdS spacetime. Whenever the dual gravitational description corresponds to Einstein gravity, the relevant surface extremizes the area functional with properly chosen boundary conditions. In the case of 1+1 dimensional theories, the EE of a spacelike interval of length ℓ is obtained through a bulk curve $\gamma(\ell)$ which extremizes the functional

$$\mathcal{F}_0[\gamma] = \mathbf{m} L[\gamma] , \tag{1.3}$$

whose endpoints correspond to those of the boundary interval. The entanglement entropy associated to the interval is given by the length of this curve i.e.

$$S_{EE}(\ell) = \mathcal{F}_0[\gamma(\ell)] , \tag{1.4}$$

for the appropriate value of \mathbf{m} . Using the gravitational duals of RG flows it is possible to construct an entropic c -function out of geodesic lengths [10].

It is often the case that the dual gravitational description of a field theory does not correspond to Einstein gravity. Indeed, as mentioned above, 1+1 dimensional conformal field theories with chiral anomalies require a modification of the bulk theory, which calls for a generalization of the RT prescription. The authors of [11] have shown that, in this context, the holographic entanglement entropy is encoded by the functional

$$\mathcal{F}[\gamma] = \mathbf{m} L[\gamma] + \mathbf{s} \int_{\gamma} \tau, \quad (1.5)$$

where τ is the extrinsic torsion of the curve γ , while \mathbf{m} and \mathbf{s} are suitably chosen constants. In the following, we would like to proceed in a similar fashion as outlined in the previous paragraph. First, we consider a boundary interval of proper length ℓ and join its endpoints (X_{\pm}, T_{\pm}) with an extremum of (1.5). Then we must elucidate how the on-shell value of (1.5) changes with ℓ in order to find the analogue of Eq. (1.2). Difficulties arise from the fact that the extrema of (1.5) correspond to Mathisson's helical motions of spinning bodies [12] which are, in general, more complicated than geodesics. Moreover, since Mathisson's helices are solutions to higher order equations, it is necessary to fix more conditions in order to single out a solution. Nevertheless, these adversities can be surmounted and in the present work we show that this geometrical problem has a succinct solution. We find that the renormalized $\mathcal{F}[\gamma]$ is given by

$$\widehat{\mathcal{F}} \equiv \ell \frac{d\mathcal{F}}{d\ell} = (T_+ - T_-) \mathcal{Q}_t + (X_+ - X_-) \mathcal{Q}_x, \quad (1.6)$$

where \mathcal{Q}_t and \mathcal{Q}_x are conserved charges associated to rigid translations of relativistic spinning bodies. Equation (1.6) is valid for any continuously varying family of Mathisson's helices connecting the interval's endpoints as we change ℓ . In general, there exist an infinite number of such families. However, at the chiral point, a natural prescription emerges that allows to select a single family of helices to which we can associate the quantity

$$\frac{c_{\text{Hel}}(\ell)}{3} \equiv \widehat{\mathcal{F}}(\ell) = \frac{\mathcal{Q}_x}{\mathcal{Q}_t}, \quad (1.7)$$

which displays the features expected by an entropic c -function for a wide variety of examples; namely, in a renormalization group flow setting, it monotonically interpolates between two CFT central charges.

2 Shape equations and anomalies

In this section we study the general properties of the extremal curves associated with the functional (1.5). The following discussion requires some acquaintance with extrinsic geometric terminology, we refer the reader to [12, 13] for a detailed discussion and notation. To describe the geometry of a curve embedded in a three-manifold we must introduce a *moving frame* comprised by a normalized tangent vector t^{μ} and two normal vectors n_A^{μ} , with

$A = 1, 2$, defined by

$$t_\mu n_A^\mu = 0 \quad g_{\mu\nu} n_A^\mu n_B^\nu = \eta_{AB}, \quad (2.1)$$

where $\eta_{AB} = \text{diag}(1, -1)$. Using this moving frame we define the extrinsic curvatures and torsion:

$$k^A = t^\mu \mathcal{D}_s n_\mu^A \quad \tau = \frac{1}{2} \epsilon_{AB} (n_\mu^A \mathcal{D}_s n^{B\mu}), \quad (2.2)$$

where $\mathcal{D}_s = t^\mu \nabla_\mu$ is the directional derivative along the curve. In terms of these quantities, the equations that dictate the shape of the extremal curves can be written as [12]

$$\mathbf{m} k_A + \mathfrak{s} \epsilon_{AB} \left[(\tilde{D}k)^B + R_s^B \right] = 0, \quad (2.3)$$

where

$$(\tilde{D}V)^A = \partial_s V^A + \tau \epsilon^{AB} \eta_{BC} V^C, \quad (2.4)$$

and

$$R_s^B = t^\mu n^{\nu B} R_{\mu\nu}. \quad (2.5)$$

Using Frenet-Serret extrinsic quantities, which are those associated with a moving frame where the extrinsic curvature in one of the normal directions is set to vanish identically, the shape equations take the convenient form:

$$\partial_s k_{\text{FS}}^2 = -2R_s^B k_B \quad k_{\text{FS}}^2 (\mathbf{m} - \mathfrak{s} \tau_{\text{FS}}) = -\mathfrak{s} \epsilon_{AB} k^A R_s^B, \quad (2.6)$$

where $k_{\text{FS}}^2 = \eta_{AB} k^A k^B$ is the total curvature and τ_{FS} is the torsion in the Frenet-Serret frame. From these equations it clearly follows that in a maximally symmetric ambient space, the total curvature is constant along extremal curves. Moreover, provided $k_{\text{FS}}^2 \neq 0$, the Frenet-Serret torsion reads

$$\tau_{\text{FS}} = \frac{\mathbf{m}}{\mathfrak{s}}, \quad (2.7)$$

and it is thus fixed by the couplings of the theory.

It is important to point out that the *shape equations* (2.3) are closely related to the Mathisson-Papapetrou-Dixon (MPD) equations [14, 15, 16]

$$\mathcal{D}_s p^\lambda = -\frac{1}{2} t^\nu \mathcal{S}^{\rho\sigma} R_{\nu\rho\sigma}^\lambda \quad (2.8)$$

$$\mathcal{D}_s \mathcal{S}^{\mu\nu} = p^\mu t^\nu - t^\mu p^\nu, \quad (2.9)$$

for the momentum p^μ and spin $\mathcal{S}^{\mu\nu}$ of an extended body in the pole-dipole approximation. The equivalence between the two systems holds only when the above are supplemented with the Mathisson-Pirani (MP) condition [17, 18]

$$\mathcal{S}^{\mu\nu} t_\mu = 0, \quad (2.10)$$

upon identifying

$$-p^\mu = \mathbf{m} t^\mu + \mathfrak{s} \epsilon_{AB} k^A n^{B\mu} \quad \mathcal{S}^{\mu\nu} = \mathfrak{s} \epsilon_{AB} n^{A\mu} n^{B\nu}. \quad (2.11)$$

Solutions $\gamma(s)$ to the system MPD with MP conditions are known in the literature as *Mathisson's helices* [19]; hereafter we use this nomenclature for the extrema of (1.5). Regarding the solutions to the shape equations (2.3) as the trajectories of spinning bodies naturally evokes concepts from dynamics. For instance, the idea that symmetries of the ambient manifold induce conserved quantities along trajectories inexorably comes to mind. Concretely, to any Killing field ξ_μ in the ambient manifold we can associate a *charge*

$$Q_\xi[\gamma] = \xi_\mu p^\mu + \frac{1}{2} \mathcal{S}^{\mu\nu} \nabla_\mu \xi_\nu, \quad (2.12)$$

which is conserved along Mathisson helices [20]. These charges will prove crucial in the arguments we develop in the forthcoming sections. It is straightforward to verify that (2.12) is conserved using the MPD equations. Nevertheless, we provide a derivation of these charges using Noether's theorem in Appendix B.

2.1 AdS₃ helices

The shape equations (2.3) can be solved analytically for maximally symmetric ambient manifolds. In [12], all possible solutions in AdS₃ spacetime,

$$ds^2 = \frac{L^2}{z^2} (\eta_{ab} dx^a dx^b + dz^2), \quad (2.13)$$

were classified in terms of their Frenet-Serret curvature k_{FS}^2 and torsion τ_{FS} . Moreover, since the Frenet-Serret torsion is fixed uniquely by the couplings of the theory ($\tau_{\text{FS}} = \mathbf{m}/\mathbf{s}$), the only free parameter is the curvature k_{FS}^2 . For the purposes of the present discussion, we are concerned with solutions which connect spacelike separated points in the boundary. This requirement imposes restrictions on the allowed values of k_{FS}^2 relative to τ_{FS} and the AdS₃ radius, either

$$0 \leq k_{\text{FS}}^2 \leq \frac{1}{L^2} - \tau_{\text{FS}}^2 \quad \text{or} \quad k_{\text{FS}}^2 \leq 0. \quad (2.14)$$

In the first case, the solution must be isometric¹ to

$$\gamma_{I_a}^\mu = \frac{L}{a \cosh \lambda_- s + b \cosh \lambda_+ s} \begin{pmatrix} a \sinh \lambda_- s \\ b \sinh \lambda_+ s \\ L \end{pmatrix}, \quad (2.15)$$

where $a^2 + L^2 = b^2$ and $a^2 \lambda_-^2 + 1 = b^2 \lambda_+^2$. In the latter instance, solutions are isometric to

$$\gamma_{I_c}^\mu = \frac{L}{a \sinh \lambda_- s + b \cosh \lambda_+ s} \begin{pmatrix} a \cosh \lambda_- s \\ b \sinh \lambda_+ s \\ L \end{pmatrix}, \quad (2.16)$$

¹Every curve with fixed k_{FS}^2 and τ_{FS} in AdS₃ can be written as the image of an AdS₃ isometry acting on a seed solution, this follows from the fundamental theorem of curves.

with $a^2 + b^2 = L^2$ and $a^2\lambda_-^2 + b^2\lambda_+^2 = 1$. In both cases we have

$$\lambda_{\pm} = \sqrt{\frac{1}{2} \left(-\Lambda \pm \sqrt{\Lambda^2 - 4 \frac{\tau_{\text{FS}}^2}{L^2}} \right)}, \quad (2.17)$$

where

$$\Lambda = k_{\text{FS}}^2 - \frac{1}{L^2} - \tau_{\text{FS}}^2. \quad (2.18)$$

Clearly, two spacelike separated points in the boundary can be joined via a bulk geodesic isometric to

$$\gamma_{\text{Geo}}^{\mu} = \begin{pmatrix} 0 \\ L \tanh(s/L) \\ L \operatorname{sech}(s/L) \end{pmatrix}, \quad (2.19)$$

which can be retrieved from either Eq. (2.15) or Eq. (2.16) by setting $\lambda_+ = 1/L$. The curves (2.15), (2.16) and (2.19) all end on boundary intervals of length $\ell = 2L$, every other boundary length can be obtained by a rescaling.

Once the extremal curves have been constructed, we must proceed to evaluate the functional (1.5) on these solutions. What makes this functional able to capture the physics of gravitational anomalies is that in contrast to the curve's length, the torsion term is not invariant under boosts [11]. Observe that the normal vectors in the moving frame (2.1) are defined up to local boosts that keep η_{AB} invariant:

$$\lambda^A_B[\psi(s)] = \begin{pmatrix} \cosh(\psi(s)) & \sinh(\psi(s)) \\ \sinh(\psi(s)) & \cosh(\psi(s)) \end{pmatrix}. \quad (2.20)$$

Under this transformation, the torsion (2.2) behaves as a gauge connection [13, 21, 22]

$$\tau(s) \rightarrow \tau(s) + \partial_s \psi(s). \quad (2.21)$$

Hence, if the functional (1.5) is evaluated on an open curve it is not necessarily invariant under gauge transformations, instead it picks up endpoint contributions

$$\mathcal{F}[\gamma] \rightarrow \mathcal{F}[\gamma] + \mathfrak{s}[\psi(s_f) - \psi(s_i)], \quad (2.22)$$

in a manner analogous to a Chern-Simons action. The crucial consequence of this observation is that to find a unique on-shell value for (1.5) it is not sufficient to fix boundary conditions for the curve but it is also necessary to impose conditions on the normal vectors. In accordance to [11] we compel the timelike normal vector to point in a predefined notion of *boundary time* at both endpoints. If instead we were to calculate the on-shell value for a κ -boosted version of the same curve, while keeping the notion of boundary time fixed, then we would need to adjust the normal frame to satisfy the boundary condition. This adjustment can be implemented by a gauge transformation satisfying $\psi(s) \rightarrow -\kappa$ at the curve's endpoints. Therefore, comparing both results we find that

$$\mathcal{F}[\Lambda(\kappa)\gamma] - \mathcal{F}[\gamma] = -2\mathfrak{s}\kappa, \quad (2.23)$$

which is a manifestation of the quantum violation of boost-invariance, a gravitational anomaly.

We wish to stress that the shape equations (2.3) are gauge covariant [12] hence the shape of the Mathisson helix itself is independent of the choice of frame. However, as mentioned before, this is not the case for the on-shell value of the functional (1.5). To illustrate this, we consider two different gauges: the Fermi-Walker gauge, where the torsion is set to zero along the entire curve, and the Frenet-Serret gauge where one of the extrinsic curvatures is set to zero identically. In the Fermi-Walker frame, the on-shell value of (1.5) reads

$$\mathcal{F}_{\text{FW}}[\gamma] = \mathbf{m} L[\gamma], \quad (2.24)$$

in contrast, for the Frenet-Serret frame we find

$$\mathcal{F}_{\text{FS}}[\gamma] = 2\mathbf{m} L[\gamma], \quad (2.25)$$

where we made use of equation (2.7). Clearly, the Frenet-Serret frame and the Fermi-Walker frame can be related by a gauge transformation. However, this must be a *large* gauge transformation ²,

$$\psi \sim \left(\frac{\mathbf{m}}{\mathbf{s}}\right) s, \quad (2.26)$$

where s is the arc-length parameter. Intuitively, this means that to go from the Frenet-Serret to Fermi-Walker frame we must *unwind* the normal frame an infinite number of times. In both cases, the answer is proportional to the length of the helix γ , which is given by

$$L[\gamma] = \frac{2}{\lambda_+} \log\left(\frac{\ell}{\epsilon}\right), \quad (2.27)$$

where ℓ is the length of the boundary interval, λ_+ is a helix parameter and ϵ is an ultraviolet cutoff. It is straightforward to check that in order to obtain the right value for the CFT computation, we must choose the Fermi-Walker frame and $\lambda_+ = 1/L$. The latter requirement implies that choosing geodesics as the extremal curve yields the right answer. In view of this fact, the reader might think that non-geodesic Mathisson's helices play no role in the study of entanglement entropy. Nonetheless, this would be a premature conclusion as we shall see in the next section.

3 Holographic RG flows

In the previous section we introduced the shape equations (2.3) and discussed some of their general properties in AdS₃ spacetime. We found that any pair of spacelike separated boundary points can be connected using a Mathisson's helix, which could be a geodesic. Now, we consider conformally flat ambient geometries which approach AdS₃ asymptotically:

$$ds^2 = \frac{L_{\text{UV}}^2}{z^2} \left(\eta_{ab} dx^a dx^b + \frac{dz^2}{f(z)^2} \right), \quad (3.1)$$

²See [23] for an interesting discussion on the subject of gauge transformations and boundary conditions.

with $f(z) \rightarrow 1$ as $z \rightarrow 0$. These spacetimes are known to provide a holographic description of the behavior of renormalization group flows [24]. The infrared ($z \rightarrow \infty$) behavior of these metrics is

$$\text{CFT}_{\text{UV}} \rightarrow \text{CFT}_{\text{IR}}, \text{ for which } f(z) \rightarrow L_{\text{UV}}/L_{\text{IR}}. \quad (3.2)$$

Spacetimes of these form are studied in detail in [25], see Appendix C. Our task is to learn how to connect space-like separated boundary points via Mathisson helices in these geometries.

We view these metrics as solutions to the equations of motion of Topologically Massive Gravity (TMG) [4] coupled to a scalar field:

$$R_{\mu\nu} - \frac{1}{2}g_{\mu\nu}R + \frac{1}{\mu}C_{\mu\nu} = 8\partial_\mu\varphi\partial_\nu\varphi - 4g_{\mu\nu}\partial^\lambda\varphi\partial_\lambda\varphi - \frac{1}{2}g_{\mu\nu}V(\varphi), \quad (3.3)$$

where

$$C_{\mu\nu} = \epsilon_\mu^{\lambda\sigma}\nabla_\lambda\left(R_{\sigma\nu} - \frac{1}{4}g_{\sigma\nu}R\right), \quad (3.4)$$

is the Cotton-York tensor. The Cotton-York tensor vanishes for conformally flat geometries, thus, in practice Eqs. (3.3) reduce to Einstein's equations. Nevertheless, we insist on regarding (3.1) in the context of TMG because the Brown-Henneaux analysis of this theory yields the central charges [5]

$$c_L = \frac{3L}{2G_3}\left(1 - \frac{1}{\mu L}\right) \quad c_R = \frac{3L}{2G_3}\left(1 + \frac{1}{\mu L}\right), \quad (3.5)$$

which signals the presence of the gravitational anomaly. In terms of the TMG couplings, the coefficients of the entangling functional (1.5) are given by

$$\mathfrak{m} = \frac{1}{4G_3} \quad \mathfrak{s} = \frac{1}{4G_3\mu}, \quad (3.6)$$

as demonstrated in [11].

For an interpolating geometry of the form (3.1), the coupling between the ambient curvature and the moving frame reads

$$R_s^A = \frac{f'(z)}{zf(z)}n^A z t^z, \quad (3.7)$$

which together with (2.6) implies that k_{FS}^2 is not necessarily constant along Mathisson helices. Hence, in contrast to the AdS_3 case, it is uncertain whether every geodesic in (3.1) can be regarded as a Mathisson helix. Indeed, since both extrinsic curvatures k^A must vanish along geodesics, for them to solve Eq. (2.3) we must have $R_s^A = 0$, which implies that either $t_s^z = 0$ or $n^{Az} = 0$. The first instance corresponds to a curve with a constant z component, that is, a curve lying on a plane parallel to the boundary. In the second case, both normal vectors are orthogonal to the z direction, which implies that the tangent vector itself is orthogonal to the boundary. Neither of this kind of geodesics can be used to connect spacelike separated points

in the boundary; the former being unable to reach the boundary and the latter touching the boundary only at one point. We conclude that to connect boundary points we are compelled to use non-geodesic Mathisson helices. Moreover, as these helices approach the boundary they should approximate either (2.15) or (2.16), up to isometries.

4 Renormalized length-torsion functional

Consider the set of spacelike boundary intervals with fixed rapidity κ and arbitrary Lorentz-invariant length ℓ in the spacetime (3.1). Assume that a prescription to construct a unique Mathisson helix $\gamma(\ell)$ connecting the endpoints of each of such intervals has been provided, see Figure 1. The question we wish to address is how does the renormalized functional

$$\widehat{\mathcal{F}}[\gamma(\ell)] = \ell \frac{\partial}{\partial \ell} \mathcal{F}[\gamma(\ell)] , \quad (4.1)$$

behave as a function of ℓ . To make progress, it is convenient to express the functional (1.5) in terms of a Lagrangian density as

$$\mathcal{F}[\gamma(\ell)] = \int_{-s_\epsilon(\ell)}^{s_\epsilon(\ell)} ds \mathcal{L}[\gamma(\ell)] , \quad (4.2)$$

with $s_\epsilon(\ell)$ defined by requiring

$$z(\pm s_\epsilon(\ell)) = \epsilon , \quad (4.3)$$

where ϵ is an ℓ -independent ultraviolet cutoff. We denote by (T_\pm, X_\pm) the endpoints of the interval, which satisfy

$$T_+ - T_- = \ell \sinh \kappa \quad X_+ - X_- = \ell \cosh \kappa , \quad (4.4)$$

by definition.

The advantage of expressing the functional (1.5) in the form (4.2) is that the ℓ derivative of $\mathcal{F}[\gamma(\ell)]$ can be separated into two distinct contributions

$$\frac{\partial \mathcal{F}}{\partial \ell} = \frac{\delta \mathcal{F}}{\delta \gamma_\mu} \frac{\partial \gamma_\mu}{\partial \ell} + \frac{\partial s_\epsilon}{\partial \ell} \mathcal{L}[\gamma(\ell)] \Big|_{-s_\epsilon}^{+s_\epsilon} . \quad (4.5)$$

The first term follows from the variation of \mathcal{F} under $\gamma^\mu \rightarrow \gamma^\mu + \delta \gamma^\mu$, which can be written as

$$\delta \mathcal{F}[\gamma] = \int_\gamma ds [\mathcal{E}^\mu \delta \gamma_\mu + \partial_s (\mathcal{J}^\mu \delta \gamma_\mu)] , \quad (4.6)$$

the explicit forms of \mathcal{E}^μ and \mathcal{J}^μ can be found in Eq. (A.5), for the present argument only some of their general properties are required. For instance, we will use the fact that $t_\mu \mathcal{E}^\mu$ vanishes identically and that

$$n_\mu^A \mathcal{E}^\mu = 0 \quad (4.7)$$

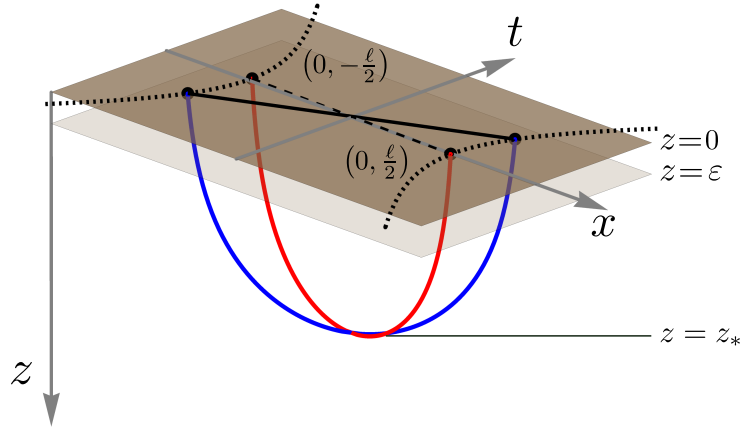


Figure 1: In the Poincaré patch of asymptotically AdS space-times, we study curves which admit a *tip* z_* , i.e. a point where $\dot{z} = 0$ and $\ddot{z} < 0$. We show two curves with identical z_* but different ζ_* : in AdS space-time, this correspond to a rigid boost, hence the endpoints of the red curve lie on the $t = 0$ line, while the blue curve endpoints are boosted. In numerical solutions, boundary quantities, such as ℓ and the boost κ , are computed at $z(s_\epsilon) = \epsilon$.

is equivalent to the shape equations (2.3). Hence, since we are considering the variation of the functional about a Mathisson helix, the first term in the right-hand side of (4.6) vanishes. Moreover, given that tangential variations of the functional correspond to reparametrizations of the curve, then

$$\mathcal{J}^\mu t_\mu = \mathcal{L}. \quad (4.8)$$

Thus, we can write (4.5) as

$$\frac{\partial \mathcal{F}}{\partial \ell} = \left[\mathcal{J}_\mu \left(t^\mu \frac{\partial s_\epsilon}{\partial \ell} + \frac{\partial \gamma^\mu}{\partial \ell} \right) \right]_{-s_\epsilon}^{+s_\epsilon}. \quad (4.9)$$

Furthermore, the endpoint values of z (which are equal to the cutoff ϵ) are independent of ℓ , consequently

$$\left. \frac{dz}{d\ell} \right|_{\pm s_\epsilon} = \left[\dot{z} \frac{\partial s_\epsilon}{\partial \ell} + \frac{\partial z}{\partial \ell} \right]_{\pm s_\epsilon} = 0, \quad (4.10)$$

and (4.9) becomes

$$\frac{\partial \mathcal{F}}{\partial \ell} = \left[\mathcal{J}_\mu \left(\frac{\partial \gamma^\mu}{\partial \ell} - \frac{\dot{\gamma}^\mu}{\dot{z}} \frac{\partial z}{\partial \ell} \right) \right]_{-s_\epsilon}^{+s_\epsilon}, \quad (4.11)$$

and it is no longer necessary to compute derivatives of s_ϵ .

Notice that as the helix γ reaches towards any of its endpoints, its shape asymptotizes to one of the AdS₃ helices described in Sec. 2.1. Interestingly, the asymptotic helices approached

at each endpoint might be distinct. As shown in Appendix D, the vector

$$\left(\frac{\partial \gamma^\mu}{\partial \ell} - \frac{\dot{\gamma}^\mu}{\dot{z}} \frac{\partial z}{\partial \ell} \right), \quad (4.12)$$

evaluated on an AdS₃ helix becomes a Killing vector which generates spacetime translations in (3.1). Variations taken along any Killing direction ξ_μ must leave the functional invariant, hence it follows from Eq. (4.6) that $\mathcal{J}^\mu \xi_\mu$ is a conserved quantity. As a matter of fact, in Appendix B we demonstrate that it matches the spinning-body conserved charge $\mathcal{Q}_\xi[\gamma]$ in equation (2.12). Bringing these facts together, it follows that the charges are bound to emerge from the contraction inside the bracket in (4.11). Finally, after dealing with a few technical details which can be found in Appendix D, we obtain the elegant expression

$$\widehat{\mathcal{F}}[\gamma(\ell)] = \ell (\mathcal{Q}_t[\gamma] \sinh \kappa + \mathcal{Q}_x[\gamma] \cosh \kappa), \quad (4.13)$$

where $\mathcal{Q}_t[\gamma]$ and $\mathcal{Q}_x[\gamma]$ are the Noether charges associated with space and time translations respectively. In particular, setting $\kappa = 0$ we have

$$\widehat{\mathcal{F}}[\gamma(\ell)] = \ell \mathcal{Q}_x[\gamma], \quad (4.14)$$

which in the limit $\mathfrak{s} \rightarrow 0$ reduces to the entropic c-function constructed in [10]. Besides translational symmetries, note that the metric (3.1) is also endowed with boost invariance. This leads to an additional Noether charge

$$\mathcal{Q}_b[\gamma] = x \mathcal{Q}_t[\gamma] + t \mathcal{Q}_x[\gamma] + \mathfrak{s} \frac{\dot{z}}{z f(z)}. \quad (4.15)$$

Interestingly, for curves that reach the asymptotic AdS boundary, and thus are Mathisson helices of the type discussed in Section 2.1, the last term is always equal to $\mathfrak{s} \lambda_+$. In the following section we will show that the relevant solutions have $\mathcal{Q}_b[\gamma] = 0$ and from the conservation of this quantity it follows that

$$\widehat{\mathcal{F}}[\gamma(\ell)] = \mathfrak{s} \lambda_+ \left(\frac{\mathcal{Q}_x[\gamma]}{\mathcal{Q}_t[\gamma]} \right), \quad (4.16)$$

provided $\mathfrak{s} \neq 0$.

5 Mathisson helices: explicit parametrization

In this section we provide an explicit parametrization to construct the Mathisson helices in an ambient spacetime of the form (3.1). In the case of AdS₃, the shape equations (2.3) can be solved following a two-step procedure. First, we solve (2.3) for the extrinsic quantities k^A and τ and with these results in hand we then construct the actual curves [12]. Due to the non-trivial coupling of the moving frame with the ambient curvature (3.7), this procedure cannot

be applied in the case of (3.1), and we are forced to introduce an explicit parametrization for the curve. As a matter of fact, the best procedure is to introduce a parametrization such that the tangent vector is automatically normalized, so that the resulting curve is parametrized by arc-length. Thus, we introduce functions $\zeta(s)$ and $\delta(s)$ such that the tangent vector reads

$$t^\mu = \frac{z}{L_{UV}} \begin{pmatrix} \sinh \zeta \\ \cos \delta \cosh \zeta \\ f(z) \sin \delta \cosh \zeta \end{pmatrix}. \quad (5.1)$$

Using (3.1) it is straightforward to verify that $t^\mu t_\mu = 1$. Next, we construct the normal frame by inverting Eqs.(2.1). Due to the gauge degeneracy in the normal bundle, we must fix a gauge beforehand in order to find a unique solution. We fix the gauge by demanding that $n^{1t} = 0$, and obtain

$$n^{1\mu} = \frac{z}{L_{UV}} \begin{pmatrix} 0 \\ \sin \delta \\ -f(z) \cos \delta \end{pmatrix} \quad n^{2\mu} = \frac{z}{L_{UV}} \begin{pmatrix} \cosh \zeta \\ \cos \delta \sinh \zeta \\ f(z) \sin \delta \sinh \zeta \end{pmatrix}, \quad (5.2)$$

for which $\eta_{AB} = \text{diag}(1, -1)$. In this frame, the curvatures and torsion read

$$k^1 = \frac{f(z)}{L_{UV}} \cos \delta + \dot{\delta} \cosh \zeta \quad k^2 = \dot{\zeta} - \frac{f(z)}{L_{UV}} \sin \delta \sinh \zeta \quad \tau = -\dot{\delta} \sinh \zeta, \quad (5.3)$$

and the shape equations (2.3) can be written as

$$\mathfrak{m} \left(\frac{f(z)}{L_{UV}} \cos \delta + \dot{\delta} \cosh \zeta \right) + \mathfrak{s} \left[\ddot{\zeta} + \cosh \zeta \left(\dot{\delta}^2 \sinh \zeta - \frac{f(z)}{L_{UV}} \dot{\zeta} \sin \delta \right) \right] = 0, \quad (5.4)$$

$$\mathfrak{m} \left(\frac{f(z)}{L_{UV}} \sin \delta \sinh \zeta - \dot{\zeta} \right) + \mathfrak{s} \left[-\cosh \zeta \ddot{\delta} + \dot{\delta} \left(\frac{f(z)}{L_{UV}} \sin \delta \cosh^2 \zeta - 2\dot{\zeta} \sinh \zeta \right) \right] = 0. \quad (5.5)$$

These equations, together with the third component of the tangent vector (5.1) make up a closed system of ordinary differential equations for $\zeta(s)$, $\delta(s)$ and $z(s)$. The x and t coordinates of the curve can be obtained by integrating the respective components of (5.1).

We construct the Mathisson helices by integrating the system of equations presented above using the *shooting method*. We choose a point in the bulk $\gamma^\mu(0) = (t_*, x_*, z_*)$ where $\dot{z}(0) = 0$, which we call the tip, from which we *shoot* towards the boundary. Observe that from (5.1) it follows that $\delta(0) = 0$. Using translational invariance we set $t_* = x_* = 0$. Clearly, these conditions are not sufficient to fix a unique solution to the shape equations, additionally we must provide a set of *shooting conditions*:

$$\left\{ \zeta_*, \dot{\delta}_*, \dot{\gamma}_* \right\}, \quad (5.6)$$

at any depth z_* , where the asterisk subscript indicates that the quantity is being evaluated at $s = 0$. Alternatively, we can use the values of the extrinsic curvatures

$$\left\{ \zeta_*, k_*^1, k_*^2 \right\}, \quad (5.7)$$

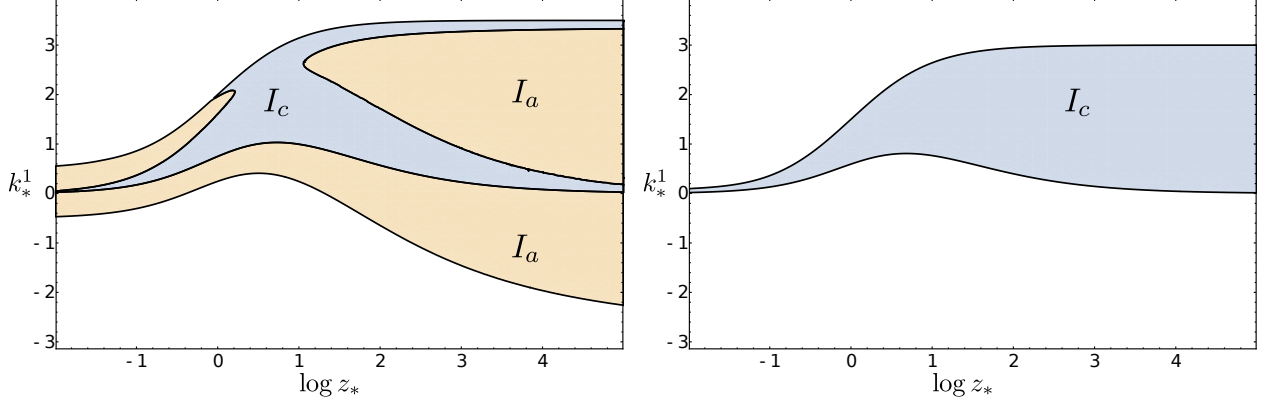


Figure 2: Example of escape regions: in the space of tip parameters z_* and k_*^1 , we show which values allow for a boundary-reaching solution. The blue/yellow color coding stand for the I_a and I_c helix types, described in (2.15) and (2.16). In this plot, we fixed for the both plots $L_{UV}/L_{IR} = 1/4$, $\mathbf{m} = 1$, $\zeta_* = 0$, $\dot{\zeta}_* = 0$. The left panel has $\mathfrak{s} = 2$, while the right one has $\mathfrak{s} = 1$. Since for the latter has $\mathbf{m}/\mathfrak{s} = 1/L_{UV}$, it represent the chiral point of the theory: notice that the absence of type I_a regions.

as shooting conditions. The data (5.6) and (5.7) can be translated into one another using

$$k_*^1 = \frac{f_*}{L_{UV}} + \dot{\delta}_* \cosh \zeta_* \quad k_*^2 = \dot{\zeta}_*. \quad (5.8)$$

In contrast to geodesics where only two parameters, depth and orientation, are needed to fix a unique solution, for Mathisson helices we must provide four. As discussed in Section 4, we are interested in helices that connect the endpoints of spacelike intervals. It is important to bear in mind that at any given depth z_* , only certain choices of shooting conditions will generate a helix that reaches the boundary in this fashion. We say that those conditions belong to the *escape region* of the model. We shall see some examples of these regions in Sec.5.1.

In the parametrization (5.1), the spinning-body Noether charges (2.12) are given by

$$\mathcal{Q}_t = -\frac{L_{UV}}{z} \left(\mathbf{m} \sinh \zeta + \mathfrak{s} \dot{\delta} \cosh^2 \zeta \right) \quad (5.9)$$

$$\mathcal{Q}_x = \frac{L_{UV}}{z} \left[\mathbf{m} \cos \delta \cosh \zeta + \mathfrak{s} \left(\dot{\delta} \cos \delta \cosh \zeta \sinh \zeta - \dot{\zeta} \sin \delta \right) \right], \quad (5.10)$$

for translational symmetries and

$$\mathcal{Q}_b = x \mathcal{Q}_t + t \mathcal{Q}_x + \mathfrak{s} \sin \delta \cosh \zeta, \quad (5.11)$$

for boosts on the (t, x) -plane. By evaluating these charges at the tip, we immediately see that $\mathcal{Q}_b = 0$, while the translational charges can be written as

$$\begin{pmatrix} \mathcal{Q}_t \\ \mathcal{Q}_x \end{pmatrix} = \frac{L_{UV}}{z_*} \begin{pmatrix} \cosh \zeta_* & -\sinh \zeta_* \\ -\sinh \zeta_* & \cosh \zeta_* \end{pmatrix} \begin{pmatrix} \mathfrak{s} (f_*/L_{UV} - k_*^1) \\ \mathbf{m} \end{pmatrix}. \quad (5.12)$$

5.1 Helical motions: numerical solutions

In this section we highlight the results from the systematic numerical study of the shape equations performed on backgrounds of the form (3.1) (and (C.1)). We construct numerical solutions for the system of equations (5.1), (5.4), and (5.5) parametrized by \mathbf{m} , \mathbf{s} , the tip depth z_* , the shooting conditions $\{\zeta_*, k_*^1, k_*^2\}$ and the parameters that determine the warp factor $f(z)$. We produce five interpolating functions:

$$\{t(s), x(s), z(s), \delta(s), \zeta(s)\}, \quad (5.13)$$

and check whether γ reaches the asymptotic boundary. Since the space-time is asymptotically AdS_3 , the solutions will necessarily approach either a I_a or I_c Mathisson helix, as we showed in Section 2.1. Each solution is unique once we fix initial conditions and parameters. In fact, we can lower the number of degrees of freedom of the solutions by imposing a few extra requirements. The first requirement is that γ should approach the *same* type of Mathisson helix on both endpoints, i.e. the solution should have identical values of λ_{\pm} asymptotically. This is equivalent in requiring that the solution should be symmetric under the change of arc-length parameter $s \rightarrow -s$, and it is easy to see that this is obtained only if $k_*^2 = 0$. Some examples of escape regions satisfying this condition are given in Figure 2. Then, in order for (4.13) to hold, all curves we consider should also have identical κ ; without loss of generality we can set $\kappa = 0$, so both endpoints lie in the $t = 0$ slice. Satisfying this condition imposes a non-trivial relationship between the three remaining tip quantities (ζ_* , z_* and k_*^1), which can be found numerically. Only after this condition is imposed, to each point in the escape region corresponds one and only one Mathisson helix. For every Mathisson helix, we then compute $\ell(z_*, k_*^1)$ and $\widehat{\mathcal{F}}(z_*, k_*^1)$. The final outputs of our algorithm are the values of these quantities over the escape regions; we present some examples in Figures 4 and 5.

Based on these findings we would like to construct *entropic c*-functions out of Mathisson's helices. Attaining this involves selecting a suitable family of Mathisson helices; in practice this correspond to delineating a properly chosen trajectory within the escape region. First of all, we require that this trajectory relates monotonically the depth z_* with the boundary width ℓ , which yields a family of curves as the one depicted in Fig. 3. Furthermore, we demand this trajectory to reproduce the expected CFT values

$$c_{\text{UV}} = 6 \mathbf{m} L_{\text{UV}} \quad \text{and} \quad c_{\text{IR}} = 6 \mathbf{m} L_{\text{IR}} \quad (5.14)$$

as $z_* \rightarrow 0$ and $z_* \rightarrow \infty$, respectively, and to interpolate between these monotonically. This means that we must select a trajectory with $k_*^1 \rightarrow 0$ in the UV as well as at the IR which crosses each contour in both plots in Fig. 4 once and only once. In general there are infinitely many ways of attaining this. However, at the chiral point, where $\mathbf{m}/\mathbf{s} = 1/L_{\text{UV}}$, the contours behave in a different manner (see Fig. 5): they either intersect the lower boundary of the escape region or continue freely towards the IR, the critical value between these two cases is precisely the contour corresponding the the expected CFT value in the IR.

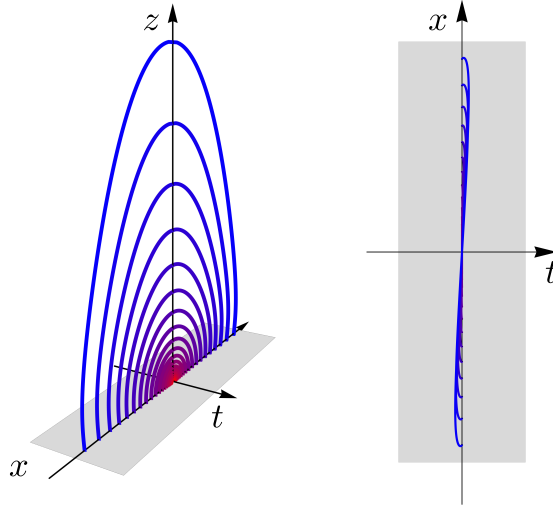


Figure 3: Graphical representation of a family of Mathisson helices, solutions of Eqs. (5.4) and (5.5). The color of each curve evolves from red to blue as z_* is increased. This family is such that the boundary boost κ is vanishing (i.e. the endpoints lie on the $t = 0$ line) and the asymptotic total curvature k_{FS}^2 is zero (so that the curves are asymptotically geodesic and end orthogonally on the boundary and have $\lambda_+ = 1$). However, these curves are *not* geodesics, and they are non planar, as is clearly seen in the vertical view on the right side of the Figure. Note that the boundary conditions $\kappa = 0$ and $\lambda_+ = 1$ can be reached only with a specific choice of tip values ζ_* and k_*^1 . This choice changes non-trivially for different z_* .

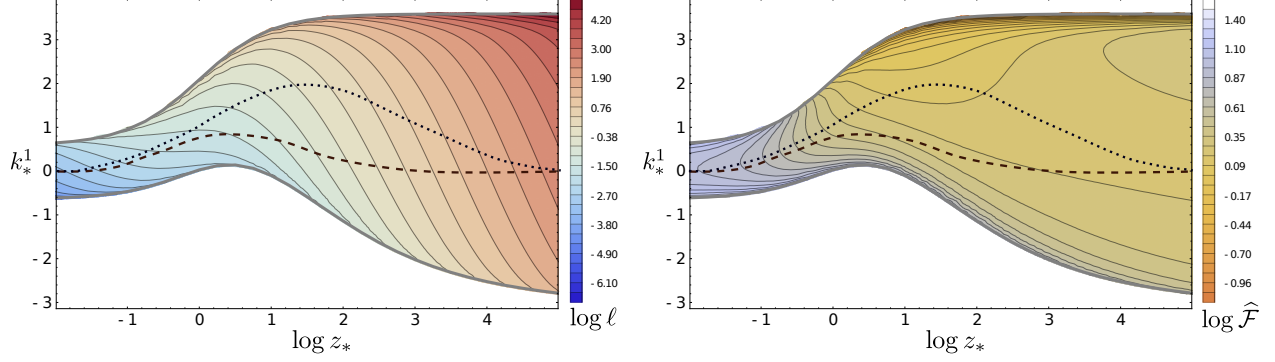


Figure 4: We take the escape region in the left panel of Figure 2, and plot logarithmic contour lines $\ell(z_*, k_*^1)$ (on the left) and $\widehat{\mathcal{F}}(z_*, k_*^1)$ (on the right). For each point within the region, we carefully tuned ζ_* so that each Mathisson helix end at the boundary with $\kappa = 0$, as in Figure 3. Within the escape region we also show two black lines, as exemplification of possible choices for curve prescriptions. The dashed (lower) black line correspond to a prescription which, as we change ℓ is also monotonic in $\widehat{\mathcal{F}}$. On the other hand, the dotted black line is an unsuitable choice because, there is a region where, for increasing ℓ , the value of $\widehat{\mathcal{F}}$ decreases (where the line crosses the same contour twice). The data in this figure has been produced choosing $L_{UV} = 1$, $L_{IR} = 1/4$, $\mathbf{m} = 1$ and $\mathfrak{s} = 2$.

Clearly, monotonicity requires that our trajectory remains below that contour. From our numerical results, we notice that as we increase the ratio L_{UV}/L_{IR} , the critical contour comes closer to the lower boundary of the escape region. Therefore, if we want to have a general prescription we must make our trajectory match the lower boundary of the escape region; this corresponds to a family of asymptotically geodesic Mathisson helices. While this choice is clearly a necessary condition for monotonicity it does not guarantee it. However, our numerical results indicate that this is the case. Thus, we propose an entropic c -function

$$\frac{c_{\text{Hel}}(\ell)}{3} = \frac{Q_x}{Q_t}, \quad (5.15)$$

at the chiral point based on the renormalized EE functional (1.5) and which can be computed entirely in terms of spinning body conserved charges. Even though the curves used to compute (5.15) are asymptotically geodesic, it is important to point out that this quantity is different to the non-anomalous case ($\mathfrak{s} = 0$). Using (4.14) and the charges (5.12), we can write

$$\widehat{\mathcal{F}} = L_{UV} \left(\frac{\ell}{z_*} \right) [\mathfrak{s} \sinh(\zeta_*) (k_*^1 - f_*/L_{UV}) + \mathbf{m} \cosh(\zeta_*)] . \quad (5.16)$$

In the non-anomalous case, extremal curves are geodesics with $\zeta_* = 0$ hence

$$\widehat{\mathcal{F}} = \frac{c_{\text{Geo}}(\ell)}{3} = \mathbf{m} L_{UV} \left(\frac{\ell}{z_*} \right), \quad (5.17)$$

which is precisely the result found in [10].

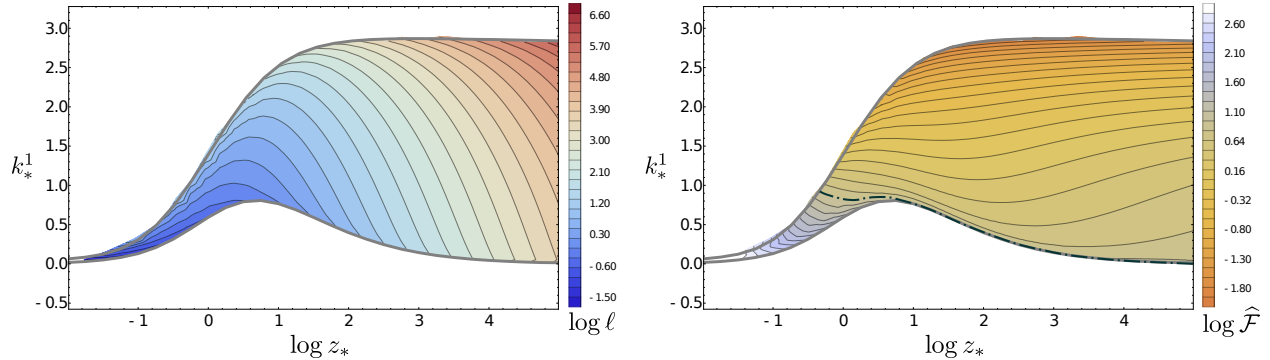


Figure 5: Similarly to Figure 4, we show the escape region at the chiral point (from the right panel of Figure 2), and plot logarithmic contour lines $\ell(z_*, k_*^1)$ (on the left) and $\widehat{\mathcal{F}}(z_*, k_*^1)$ (on the right). Note that the vertical axis has been rescaled. In the right panel, highlight with a dot-dashed black line the limiting level set of $\widehat{\mathcal{F}}$ that separates contour lines ending on the lower boundary of the escape region from contour lines that eventually will reach the upper boundary. The value of $\widehat{\mathcal{F}}$ along this line is precisely the infrared CFT value of the central charge: therefore, monotonicity requires that a prescription line (such as the black dotted/dashed lines in Figure 4) has to lie below this limiting contour.

6 Discussion and outlook

In this work we have explored the physical properties of the length-torsion functional (1.5). As demonstrated in [11], this functional computes holographically the entanglement entropy for 1+1 dimensional theories with chiral anomalies. Moreover, in a previous paper [12] we have shown that the extremal curves of this functional correspond to Mathisson’s helical motions for the centers of mass of spinning bodies. Here, we have brought together these two points of view and constructed an entropic c -function $c_{\text{Hel}}(\ell)$ which can be written in terms of Noether charges along Mathisson’s helices. While for generic values of the anomaly there is some ambiguity in the definition of $c_{\text{Hel}}(\ell)$, we argued that at the chiral point (1.1) this ambiguity is absent. Indeed, at the chiral point we find the succinct expression (5.15) which must be evaluated on asymptotically geodesic Mathisson helices. We have gathered extensive numerical evidence in support of the monotonicity of this function, we leave the derivation of a formal proof of this fact for future work.

We wish to point out that the steps leading to the expressions for the renormalized functional, Eqs.(4.13) and (4.16), relied only on the assumption of having an AdS_3 asymptopia. Hence, these expressions can be used without any modification for any IR behavior one might wish to study, such as warped AdS_3 , Janus or gapped geometries. Indeed, for the case of gapped geometries we will detail in a forthcoming work how Mathisson helices prevent the formation of mass gaps which are precluded by anomaly matching, see [26] for a general argument. Another intriguing direction is to revisit entanglement entropy for theories with different symmetry algebras and whose gravitational duals are naturally understood in

the realm of TMG such as Galilean CFTs, see for instance [27] and [28]. On a more ludic note, when exploring the space of Mathisson helices in domain walls, we noticed that beyond the regions of existence there are also groups of minute escape regions in parameter space which allow for an interesting kind of solutions: helices in those regions escape towards the boundary only after traveling deeper into the bulk and gathering enough momentum from the spin-curvature interaction. It would be amusing to explore what these solutions might be able to teach us. Finally, we wish to understand the results discussed in this work from a field theoretic standpoint. First, it would be desirable to obtain a CFT picture of Mathisson's helices and their charges. Based on this, we ought to be able to translate $c_{\text{Hel}}(\ell)$ into the language of the dual theory. Presumably, this would allow us to make contact with the very interesting literature concerning EE in CFTs with chiral anomalies, [29, 30, 31, 32].

Acknowledgements

PF is supported by the Netherlands Organisation for Scientific Research (NWO/OCW). The work of AVO is supported by the NCN grant 2012/06/A/ST2/00396. AVO wishes to thank the Yukawa Institute for Theoretical Physics for hospitality during the development of this work. Also, AVO is grateful to Abdus Salam International Center for Theoretical Physics where he carried out some of the final stages of this project. It is a pleasure to acknowledge Michael Abbott, Paweł Caputa, Alejandra Castro, Filipe Costa, Mario Flory, Vishnu Jejjala and José Natario for enlightening conversations and correspondence. We thank Alejandra Castro, Mario Flory, Vishnu Jejjala and Hesam Soltanpanahi for helpful comments on earlier versions of this work. Especially, we wish to express our gratitude to Alejandra Castro for suggesting us to look into these questions.

A Helical Noether charges

In this Appendix we show how the quantity (2.12) can be derived from the action (1.5) by means of Noether's theorem.

Since $\{t^\mu, n^{1\mu}, n^{2\mu}\}$ form an oriented basis frame in the neighbourhood of the curve, we can decompose any (Killing) vector field ξ^μ defined on TM in its components. Explicitly we thus have

$$\xi^\mu = \xi_t t^\mu + \xi_A n^{A\mu}, \quad (\text{A.1})$$

where ξ_t and ξ_A are respectively the tangential and normal components of the Killing vector field.

Note that the expression written in (2.12) is gauge invariant, i.e. does not depend on any particular choice of the curve's normal frame. For this reason, it is convenient to (tem-

porarily) make (1.5) also gauge invariant by adding a *compensator*:

$$\tilde{\mathcal{F}}[\gamma] \equiv \int_{\Sigma} ds \left(\mathbf{m} + \mathfrak{s} \left(\tau - \dot{\psi} \right) \right), \quad (\text{A.2})$$

where $\psi(s)$ is the hyperbolic angle of $n^{1\mu}$ with any arbitrarily fixed normal frame. For example, we can choose ψ to be the angle with the Fermi-Walker gauge choice, so that *if and only if* we compute geometrical quantities in this frame, we can set $\psi = 0$. Under a local frame rotation the compensator term changes in exactly the opposite way as τ , rendering (A.2) effectively gauge invariant. The compensator arises also in the evaluation of some connection forms, namely

$$\frac{1}{2} \epsilon_{AB} n^{A\mu} n^{B\nu} \nabla_{\mu} t_{\nu} = \tau - \dot{\psi}, \quad (\text{A.3})$$

being the l.h.s of this expression a well-behaved scalar.

We can now substitute (A.1) into (2.12), finding

$$\mathcal{Q}_{\xi}[\gamma] = \xi_t \left(\mathbf{m} + \mathfrak{s} \left(\tau - \dot{\psi} \right) \right) - \mathfrak{s} \epsilon_{AB} \left(\xi^A \text{Tr} K^B + \frac{1}{2} n^{A\mu} \nabla_{\mu} \xi^B + \frac{1}{2} \xi_C \Theta^{ACB} \right). \quad (\text{A.4})$$

On the other hand, by taking an on-shell Lie derivative of (A.2) along the vector field (A.1), we get

$$\mathcal{L}_{\xi} \tilde{\mathcal{F}}[\gamma] = \left[\xi_t \left(\mathbf{m} + \mathfrak{s} \left(\tau - \dot{\psi} \right) \right) - \mathfrak{s} \epsilon_{AB} \left(\xi^A \text{Tr} K^B - \frac{1}{2} \xi_C \Theta^{CBA} \right) \right]_{s=\pm\infty}. \quad (\text{A.5})$$

To obtain the above result we used the fact that the bulk of the variation is zero because of the shape equations, and used the fact that $\mathcal{L}_{\xi} \psi = 0$ at the boundary. Because of Noether's theorem, if ξ^{μ} is a Killing vector field, being (A.2) a geometrical invariant action (i.e. it does not depend on coordinate choices), then the term inside the brackets of (A.5) and expression (A.4) should match.

In order to prove the equivalence of the two expressions, we need to use the fact that Killing vectors preserve orthonormal frames. In particular, the normal vectors can be Lie-transported along any space-time Killing directions

$$\mathcal{L}_{\xi} n^{B\mu} = \xi^{\nu} \nabla_{\nu} n^{B\mu} - n^{B\nu} \nabla_{\nu} \xi^{\mu} = 0. \quad (\text{A.6})$$

By contracting the above expression with $\epsilon_{AB} n_{\nu}^A$ we get the relation

$$\epsilon_{AB} \left(\xi_C \Theta^{CAB} - n^{A\mu} \nabla_{\mu} \xi^B - \xi_C \Theta^{ACB} \right) = 0, \quad (\text{A.7})$$

which, upon using $\xi_C \Theta^{C[AB]} = 0$, proves the equivalence between (A.4) and (A.5).

B Spinning-body charges in AdS₃

In the following, we compute the conserved charges of helices isometric to (2.15) or (2.16) in AdS₃. Specifically, we will be interested in helices of the form

$$\gamma = \frac{r}{2L_{UV}} M^\mu{}_\nu x^\nu + \Delta^\mu, \quad (\text{B.1})$$

where x^ν is either $\gamma_{I_a}^\mu$ or $\gamma_{I_c}^\mu$, $r/2L_{UV}$ is a dilatation corresponding to a boundary interval length $\ell = r$ and, $M^\mu{}_\nu$ and Δ^μ are the boost and the translation

$$M^\mu{}_\nu = \begin{pmatrix} \cosh(\eta) & -\sinh(\eta) & 0 \\ -\sinh(\eta) & \cosh(\eta) & 0 \\ 0 & 0 & 1 \end{pmatrix} \quad \Delta^\mu = \begin{pmatrix} \Delta^t \\ \Delta^x \\ 0 \end{pmatrix}. \quad (\text{B.2})$$

A simple approach to compute these charges is to regard the ambient space as a hypersurface embedded in a four-dimensional flat space described as the zero set of $y^\alpha y_\alpha + L^2$ in \mathbb{R}^4 , endowed with the metric $\text{diag}(-, -, +, +)$. The map we use for the embedding is

$$(t, x, z) = \frac{L}{y^1 + y^4} (y^2, y^3, L) \quad (\text{B.3})$$

with inverse mapping

$$(y^1, y^2, y^3, y^4) = \frac{1}{2z} (L^2 - t^2 + x^2 + z^2, 2Lt, 2Lx, L^2 + t^2 - x^2 - z^2). \quad (\text{B.4})$$

As a first step, we find the Killing vectors associated to the charges \mathcal{Q}_t , \mathcal{Q}_x and \mathcal{Q}_b . A simple coordinate transformation yields the results

$$\xi_t^\mu = \frac{1}{L_{UV}} (-y^2, y^1 + y^4, 0, y^2) \quad \xi_x^\mu = \frac{1}{L_{UV}} (y^3, 0, y^1 + y^4, -y^3) \quad \xi_b^\mu = (0, y^3, y^2, 0). \quad (\text{B.5})$$

To compute \mathcal{Q}_t and \mathcal{Q}_x we use the FS frame to calculate the momentum p^μ and spin $S^{\mu\nu}$ of the curve. This is a rather complicated task on the Poincaré patch of AdS, the key difficulty lies on the fact that \mathcal{D}_s is not an ordinary derivative. To circumvent this complication, we compute these quantities in the hyperbolic submanifold, where the FS frame equations are linear due to the fact that the directional derivative is given by

$$\mathcal{D}_s V^\alpha = \partial_s V^\alpha + \frac{1}{L_{UV}^2} (y_\beta \partial_s V^\beta) y^\alpha \quad (\text{B.6})$$

To further simplify the computations, we take Δ^μ to be zero, since \mathcal{Q}_t and \mathcal{Q}_x do not depend on (t, x) -plane translations. The resulting charges are

$$\begin{pmatrix} \mathcal{Q}_t \\ \mathcal{Q}_x \end{pmatrix} = \frac{2L_{UV}}{r} \begin{pmatrix} \cosh(\eta) & \sinh(\eta) \\ \sinh(\eta) & \cosh(\eta) \end{pmatrix} \begin{pmatrix} \mathfrak{s}\lambda_+ \\ \mathfrak{s}\lambda_- \end{pmatrix}. \quad (\text{B.7})$$

Finally, to compute \mathcal{Q}_b we use fact that

$$\sin [\delta(s)] \cosh [\zeta(s)] = \frac{L_{UV} t^z(s)}{zf(z)}, \quad (\text{B.8})$$

from which we find that

$$\mathcal{Q}_b = \mathcal{Q}_x \Delta^t + \mathcal{Q}_t \Delta^x, \quad (\text{B.9})$$

Notice that when Q_b is zero, this equation implies

$$\mathcal{Q}_t \Delta^x = -\mathcal{Q}_x \Delta^t \quad (\text{B.10})$$

C Holographic RG Flow Between 2d CFTs

The metrics that we employ in our numerical analysis are analytic domain wall solution of three-dimensional $SO(4) \times SO(4)$ gauged supergravity constructed in [25], which correspond to supersymmetric RG flows between conformal field theories. This metric can be written in the form

$$ds^2 = e^{-2A(\rho)} \eta_{ab} dx^a dx^b + d\rho^2, \quad (\text{C.1})$$

with

$$A(\rho) = \frac{\alpha}{2\beta} \rho - \frac{1}{2} \log \left[\text{sech} \left(\frac{\rho}{\beta} \right) \right], \quad (\text{C.2})$$

where

$$\alpha = \frac{L_{IR} + L_{UV}}{L_{UV} - L_{IR}}, \quad \beta = \frac{L_{IR} L_{UV}}{L_{UV} - L_{IR}}. \quad (\text{C.3})$$

Since this metric is given in a different coordinate system than Eq. (3.1), for the readers convenience we reproduce some of the basic formulas of Sec. 5 below.

We use the following parametrization to describe the curve:

$$t^\mu = \begin{pmatrix} e^{A(\rho)} \sinh \zeta \\ e^{A(\rho)} \cos \delta \cosh \zeta \\ \sin \delta \cosh \zeta \end{pmatrix}, \quad (\text{C.4})$$

with orthogonal frame

$$n^{1\mu} = \begin{pmatrix} 0 \\ e^{A(\rho)} \sin \delta \\ -\cos \delta \end{pmatrix} \quad n^{2\mu} = \begin{pmatrix} e^{A(\rho)} \cosh \zeta \\ e^{A(\rho)} \cos \delta \sinh \zeta \\ \sin \delta \sinh \zeta \end{pmatrix} \quad (\text{C.5})$$

The curvatures and torsion associated to the frame are

$$k^1 = A'(\rho) \cos \delta + \dot{\delta} \cosh \zeta \quad k^2 = \dot{\zeta} - A'(\rho) \sin \delta \sinh \zeta \quad \tau = -\dot{\delta} \sinh \zeta. \quad (\text{C.6})$$

The shape equations are given by

$$\mathbf{m} \left(A'(\rho) \cos \delta + \dot{\delta} \cosh \zeta \right) + \mathfrak{s} \left[\ddot{\zeta} + \cosh \zeta \left(\dot{\delta}^2 \sinh \zeta - A'(\rho) \dot{\zeta} \sin \delta \right) \right] = 0 \quad (\text{C.7})$$

$$\mathbf{m} \left(A'(\rho) \sin \delta \sinh \zeta - \dot{\zeta} \right) + \mathfrak{s} \left[-\cosh \zeta \ddot{\delta} + \dot{\delta} \left(A'(\rho) \sin \delta \cosh^2 \zeta - 2\dot{\zeta} \sinh \zeta \right) \right] = 0 \quad (\text{C.8})$$

Notice that the shape equations, the curvatures, and the torsion only change by $f(z)/L_{\text{UV}} \rightarrow A'(\rho)$.

If we impose the condition $\dot{\rho}(0) = 0$, with fixed values for ρ_* , ζ_* , k_*^1 and k_*^2 we get the following tip conditions

$$\delta_* = 0 \quad \dot{\delta}_* = \text{sech}(\zeta_*) (k_*^1 - A'(\rho_*)) \quad \dot{\zeta}_* = k_*^2 \quad (\text{C.9})$$

We have the same three Killing vectors ξ_t , ξ_x and ξ_b . The corresponding charges are

$$\mathcal{Q}_t = -e^{-A(\rho)} \left(\mathbf{m} \sinh \zeta + \mathfrak{s} \dot{\delta} \cosh^2 \zeta \right) \quad (\text{C.10})$$

$$\mathcal{Q}_x = e^{-A(\rho)} \left[\mathbf{m} \cos \delta \cosh \zeta + \mathfrak{s} \left(\dot{\delta} \cos \delta \cosh \zeta \sinh \zeta - \dot{\zeta} \sin \delta \right) \right] \quad (\text{C.11})$$

$$\mathcal{Q}_b = x \mathcal{Q}_t + t \mathcal{Q}_x + \sigma \cosh \zeta \sin \delta \quad (\text{C.12})$$

Evaluating the charges at the tip, they can be written as:

$$\begin{pmatrix} \mathcal{Q}_t \\ \mathcal{Q}_x \end{pmatrix} = e^{-A_*} \begin{pmatrix} \cosh \zeta_* & -\sinh \zeta_* \\ -\sinh \zeta_* & \cosh \zeta_* \end{pmatrix} \begin{pmatrix} \mathfrak{s}(A'_* - k_*^1) \\ \mathbf{m} \end{pmatrix}, \quad (\text{C.13})$$

while we notice from the initial conditions that $\mathcal{Q}_b = 0$.

D Matching charges

In this section, we connect the Mathisson helices behavior at the boundary with the parameters that define them on the tip, with the objective to prove equation (4.13). For this purpose, we exploit the fact that solutions to the shape equations (2.3) become asymptotically the AdS₃ ones, whose solutions are the helices (B.1) discussed in appendix B. In what follows, we will use the same definitions for r , η , Δ^t and Δ^x , but we will add a superscript (\pm) to each of these parameters, to take into account that there might be different asymptotic helices for each of the curves endpoints.

We start by using the conserved charges \mathcal{Q}_t , \mathcal{Q}_x expressed in two different ways using tip (5.10) and boundary (B.7) quantities. By equating the expressions, we find the following

relations for the dilatations $r^{(\pm)}$ and boost parameters $\eta^{(\pm)}$

$$r^{(\pm)} = 2\mathfrak{s}z_* \sqrt{\frac{(\lambda_+^{(\pm)})^2 - (\lambda_-^{(\pm)})^2}{\mathfrak{s}^2 \dot{\delta}_*^2 \cosh(\zeta_*)^2 - \mathfrak{m}^2}}, \quad (\text{D.1})$$

$$\eta^{(\pm)} = -\zeta_* + \frac{1}{2} \log \left[\frac{(\mathfrak{s} \dot{\delta}_* \cosh \zeta_* - \mathfrak{m}) (\lambda_+^{(\pm)} - \lambda_-^{(\pm)})}{(\mathfrak{s} \dot{\delta}_* \cosh \zeta_* + \mathfrak{m}) (\lambda_+^{(\pm)} + \lambda_-^{(\pm)})} \right] \quad (\text{D.2})$$

For the case of \mathcal{Q}_b , tip conditions imply that its value is zero, so

$$\mathcal{Q}_x (\Delta^t)^{(\pm)} = -\mathcal{Q}_t (\Delta^x)^{(\pm)}. \quad (\text{D.3})$$

The significance of these relations is that we can use them to find the length ℓ and the rapidity κ of the interval bounded by endpoints (T_{\pm}, X_{\pm}) . Moreover, we can use the parametrization of the AdS₃ helices to find an expression for this endpoints. For helices isometric to $\gamma_{I_a}^{\mu}$ or $\gamma_{I_c}^{\mu}$, we find that

$$T_{\pm} = (\Delta^t)^{(\pm)} \mp r^{(\pm)} \sinh(\eta^{(\pm)}) \quad (\text{D.4})$$

$$X_{\pm} = (\Delta^t)^{(\pm)} \pm r^{(\pm)} \cosh(\eta^{(\pm)}). \quad (\text{D.5})$$

Using these relations and equation (4.4) we get

$$(\Delta^t)^{(+)} - (\Delta^t)^{(-)} = \ell \sinh \kappa + \frac{1}{2} (r^{(+)} \sinh \eta^{(+)} + r^{(-)} \sinh \eta^{(-)}) \quad (\text{D.6})$$

$$(\Delta^x)^{(+)} - (\Delta^x)^{(-)} = \ell \cosh \kappa - \frac{1}{2} (r^{(+)} \cosh \eta^{(+)} + r^{(-)} \cosh \eta^{(-)}). \quad (\text{D.7})$$

By substituting the relations (D.6) and (D.7) into (4.12) we find that

$$\left[\frac{\partial \gamma^{\mu}}{\partial \ell} - \frac{\dot{\gamma}^{\mu}}{\dot{z}} \frac{\partial z}{\partial \ell} \right]_{-s_{\epsilon}}^{+s_{\epsilon}} = \begin{pmatrix} \sinh \kappa \\ \cosh \kappa \\ 0 \end{pmatrix}, \quad (\text{D.8})$$

and therefore

$$\widehat{\mathcal{F}}[\gamma(\ell)] = \ell(\mathcal{Q}_t[\gamma] \sinh \kappa + \mathcal{Q}_x[\gamma] \cosh \kappa). \quad (\text{D.9})$$

References

- [1] A. B. Zamolodchikov, “Irreversibility of the Flux of the Renormalization Group in a 2D Field Theory”, *JETP Lett.* **43** (1986) 730–732, [Pisma Zh. Eksp. Teor. Fiz.43,565(1986)].
- [2] F. Bastianelli and U. Lindstrom, “C theorem for two-dimensional chiral theories”, *Phys. Lett.* **B380** (1996) 341–345, [arXiv:hep-th/9604001](#).
- [3] J. D. Brown and M. Henneaux, “Central Charges in the Canonical Realization of Asymptotic Symmetries: An Example from Three-Dimensional Gravity”, *Commun. Math. Phys.* **104** (1986) 207–226.
- [4] S. Deser, R. Jackiw, and S. Templeton, “Three-Dimensional Massive Gauge Theories”, *Phys. Rev. Lett.* **48** (1982) 975–978.
- [5] K. Hotta, Y. Hyakutake, T. Kubota, and H. Tanida, “Brown-Henneaux’s Canonical Approach to Topologically Massive Gravity”, *JHEP* **07** (2008) 066, [arXiv:0805.2005](#).
- [6] W. Li, W. Song, and A. Strominger, “Chiral gravity in three dimensions”, *Journal of High Energy Physics* **2008** apr (2008) 082–082, [0801.4566](#).
- [7] H. Casini and M. Huerta, “A Finite entanglement entropy and the c-theorem”, *Phys. Lett.* **B600** (2004) 142–150, [arXiv:hep-th/0405111](#).
- [8] H. Liu and M. Mezei, “A Refinement of entanglement entropy and the number of degrees of freedom”, *JHEP* **04** (2013) 162, [arXiv:1202.2070](#).
- [9] S. Ryu and T. Takayanagi, “Holographic derivation of entanglement entropy from AdS/CFT”, *Phys. Rev. Lett.* **96** (2006) 181602, [arXiv:hep-th/0603001](#).
- [10] R. C. Myers and A. Singh, “Comments on Holographic Entanglement Entropy and RG Flows”, *JHEP* **04** (2012) 122, [arXiv:1202.2068](#).
- [11] A. Castro, S. Detournay, N. Iqbal, and E. Perlmutter, “Holographic entanglement entropy and gravitational anomalies”, *JHEP* **07** (2014) 114, [arXiv:1405.2792](#).
- [12] P. Fonda, D. Liska, and A. Veliz-Osorio, “Spinning probes and helices in AdS₃”, [arXiv:1803.05283](#).
- [13] P. Fonda, V. Jejjala, and A. Veliz-Osorio, “On the Shape of Things: From holography to elastica”, *Annals Phys.* **385** (2017) 358–398, [arXiv:1611.03462](#).
- [14] M. Mathisson, “Neue mechanik materieller systemes”, *Acta Phys. Polon.* **6** (1937) 163–2900.

- [15] A. Papapetrou, “Spinning test particles in general relativity. 1.”, *Proc. Roy. Soc. Lond.* **A209** (1951) 248–258.
- [16] W. G. Dixon, “Dynamics of extended bodies in general relativity. II. Moments of the charge-current vector”, *Proc. Roy. Soc. Lond.* **A319** (1970) 509–547.
- [17] M. Mathisson, “Das zitternde Elektron und seine Dynamik”, *Acta Phys. Polon.* **6** (1937) 218–227.
- [18] F. A. E. Pirani, “On the Physical significance of the Riemann tensor”, *Acta Phys. Polon.* **15** (1956) 389–405, [Gen. Rel. Grav.41,1215(2009)].
- [19] F. Costa, C. A. R. Herdeiro, J. Natario, and M. Zilhao, “Mathisson’s helical motions for a spinning particle: Are they unphysical?”, *Phys. Rev.* **D85** (2012) 024001, [arXiv:1109.1019](#).
- [20] R. Hojman and S. Hojman, “Spinning Charged Test Particles in a Kerr-Newman Background”, *Phys. Rev.* **D15** (1977) 2724.
- [21] R. Capovilla and J. Guven, “Geometry of deformations of relativistic membranes”, *Phys. Rev.* **D51** (1995) 6736–6743, [arXiv:gr-qc/9411060](#).
- [22] B. Carter, “Essentials of classical brane dynamics”, *Int. J. Theor. Phys.* **40** (2001) 2099–2130, [arXiv:gr-qc/0012036](#).
- [23] M. Bañados and I. A. Reyes, “A short review on Noethers theorems, gauge symmetries and boundary terms”, *Int. J. Mod. Phys.* **D25** (2016), no. 10, 1630021, [arXiv:1601.03616](#).
- [24] J. de Boer, E. P. Verlinde, and H. L. Verlinde, “On the holographic renormalization group”, *JHEP* **08** (2000) 003, [arXiv:hep-th/9912012](#).
- [25] M. Berg and H. Samtleben, “An Exact holographic RG flow between 2-d conformal fixed points”, *JHEP* **05** (2002) 006, [arXiv:hep-th/0112154](#).
- [26] A. Belin, A. Castro, and L.-Y. Hung, “Fake gaps in $\text{AdS}_3/\text{CFT}_2$ ”, *JHEP* **11** (2015) 145, [arXiv:1508.01201](#).
- [27] A. Bagchi, R. Basu, D. Grumiller, and M. Riegler, “Entanglement entropy in Galilean conformal field theories and flat holography”, *Phys. Rev. Lett.* **114** (2015), no. 11, 111602, [arXiv:1410.4089](#).
- [28] S. M. Hosseini and A. Véliz-Ororio, “Gravitational anomalies, entanglement entropy, and flat-space holography”, *Phys. Rev.* **D93** (2016), no. 4, 046005, [arXiv:1507.06625](#).
- [29] T. Azeyanagi, R. Loganayagam, and G. S. Ng, “Anomalies, Chern-Simons Terms and Black Hole Entropy”, *JHEP* **09** (2015) 121, [arXiv:1505.02816](#).

- [30] T. Nishioka and A. Yarom, “Anomalies and Entanglement Entropy”, *JHEP* **03** (2016) 077, [arXiv:1509.04288](#).
- [31] N. Iqbal and A. C. Wall, “Anomalies of the Entanglement Entropy in Chiral Theories”, *JHEP* **10** (2016) 111, [arXiv:1509.04325](#).
- [32] T. L. Hughes, R. G. Leigh, O. Parrikar, and S. T. Ramamurthy, “Entanglement entropy and anomaly inflow”, *Phys. Rev.* **D93** (2016), no. 6, 065059, [arXiv:1509.04969](#).